Clay hypoplasticity model including stiffness anisotropy

David Mašín

corresponence address:
Charles University in Prague
Faculty of Science
Albertov 6
12843 Prague 2, Czech Republic
E-mail: masin@natur.cuni.cz
Tel: +420-2-2195 1552, Fax: +420-2-2195 1556

Submitted for publication in Géotechnique
Article type: Technical Note
Number of words main text: 1844
Number of words other parts: 607 (references), 289 (appendix), 83 (abstract).
Nov 26 2013

Abstract

Hypoplastic model for clays is developed predicting anisotropy of very small strain stiffness. The existing hypoplastic model with explicit formulation of the asymptotic state boundary surface is combined with an anisotropic form of the stiffness tensor. Naturally, the resultant model predicts correctly the very small strain stiffness anisotropy. It is demonstrated that properly are also predicted trends in the anisotropy influence on undrained stress paths. The model is evaluated using hollow cylinder apparatus experimental data on London clay taken over from literature.

Keywords: clays; anisotropy; constitutive relations; stiffness; stress path

Introduction

Anisotropy of sedimentary clays is such a significant feature of their mechanical behaviour that it cannot be ignored in boundary value problem simulations. For example, Addenbrooke et al. (1997), Gunn (1993), Ng et al. (2004) and Franzius et al. (2005) demonstrated that incorporation of stiffness anisotropy improved predictions of tunnelling problems. In this Note, we develop a hypoplastic model for clays incorporating very small strain stiffness anisotropy. Like the underlining hypoplastic models, the model is capable of predicting small strain stiffness non-linearity, recent stress history effects (Atkinson et al. 1990) and large-strain asymptotic behaviour (Gudehus and Mašín 2009, Mašín 2012a). The model is based on the earlier research by the author, which will only briefly be summarised here due to limitted space. For details of hypoplastic modelling, the readers are referred to the cited publications.

Hypoplasticity is an approach to non-linear constitutive modelling of geomaterials. In its general form by (Gudehus 1996) it may be written as

$$\mathring{\boldsymbol{\sigma}} = f_s(\boldsymbol{\mathcal{L}} : \dot{\boldsymbol{\epsilon}} + f_d \mathbf{N} \|\dot{\boldsymbol{\epsilon}}\|) \tag{1}$$

where $\mathring{\boldsymbol{\sigma}}$ and $\dot{\boldsymbol{\epsilon}}$ represent the objective (Zaremba-Jaumann) stress rate and the Euler stretching tensor respectively, $\boldsymbol{\mathcal{L}}$ and $\mathbf{N}$ are fourth- and second-order constitutive tensors, and f_s and f_d are two scalar factors. In hypoplasticity, stiffness predicted by the model is controlled by the tensor $\boldsymbol{\mathcal{L}}$, while strength (and asymptotic response in general, see Mašín (2012a), is governed by a combination of $\boldsymbol{\mathcal{L}}$ and $\mathbf{N}$. Earlier hypoplastic models (such as the model by Wolffersdorff 1996 and Mašín 2005) did not allow to change the $\boldsymbol{\mathcal{L}}$ formulation arbitrarily, as any modification of the tensor $\boldsymbol{\mathcal{L}}$ undesirably influenced the predicted asymptotic states. This hypoplasticity limitation was overcome by Mašín (2012c). He developed an approach enabling to specify the asymptotic state boundary surface independently of the tensor $\boldsymbol{\mathcal{L}}$ and demonstrated it by proposing a simple hypoplastic equivalent of the Modified Cam-clay model. Based this approach, Mašín (2012b) developed an advanced hypoplastic model for clays. This model will serve as a base model for current developments.

Model formulation

The model presented in this Note combines hypoplastic model from Mašín (2012b) with anisotropic form of the tensor $\boldsymbol{\mathcal{L}}$ proposed by Mašín and Rott (2013)[1]. Mašín and Rott (2013) adopted general transversely elastic model formulation, which reads (Spencer 1982, Lubarda and Chen 2008)

$$\boldsymbol{\mathcal{L}} = \frac{1}{2} a_1 \mathbf{1} \circ \mathbf{1} + a_2 \mathbf{1} \otimes \mathbf{1} + a_3 \left(\mathbf{p} \otimes \mathbf{1} + \mathbf{1} \otimes \mathbf{p}\right) + a_4 \mathbf{p} \circ \mathbf{1} + a_5 \mathbf{p} \otimes \mathbf{p} \tag{2}$$

where the tensor products represented by "⊗" and "∘" are defined as

$$(\mathbf{p} \otimes \mathbf{1})_{ijkl} = p_{ij} 1_{kl} \qquad (\mathbf{p} \circ \mathbf{1})_{ijkl} = \frac{1}{2}\left(p_{ik} 1_{jl} + p_{il} 1_{jk} + p_{jl} 1_{ik} + p_{jk} 1_{il}\right) \tag{3}$$

where $p_{ij} = n_i n_j$; n_i is a unit vector normal to the plane of symmetry (in sedimentary soils this vector typically represents the vertical direction). a_1 to a_5 in Eq. (2) represent five material constants. They can be calculated as

$$a_1 = \alpha_E \left(1 - \nu_{pp} - 2 \frac{\alpha_E}{\alpha_\nu^2} \nu_{pp}^2\right) \tag{4}$$

$$a_2 = \alpha_E \nu_{pp} \left(1 + \frac{\alpha_E}{\alpha_\nu^2} \nu_{pp}\right) \tag{5}$$

$$a_3 = \alpha_E \nu_{pp} \left(\frac{1}{\alpha_\nu} + \frac{\nu_{pp}}{\alpha_\nu} - 1 - \frac{\alpha_E}{\alpha_\nu^2} \nu_{pp}\right) \tag{6}$$

[1] Similar problem has already been discussed by Kopito and Klar (2013), who incorporated transversely isotropic stiffness tensor $\boldsymbol{\mathcal{L}}$ into the model by Mašín (2012c).

$$a_4 = \alpha_E \left(1 - \nu_{pp} - 2\frac{\alpha_E}{\alpha_\nu^2}\nu_{pp}^2\right)\frac{1-\alpha_G}{\alpha_G} \tag{7}$$

$$a_5 = \alpha_E \left(1 - \frac{\alpha_E}{\alpha_\nu^2}\nu_{pp}^2\right) + 1 - \nu_{pp}^2 - 2\frac{\alpha_E}{\alpha_\nu}\nu_{pp}\left(1 + \nu_{pp}\right) - \frac{2\alpha_E}{\alpha_G}\left(1 - \nu_{pp} - 2\frac{\alpha_E}{\alpha_\nu^2}\nu_{pp}^2\right) \tag{8}$$

where the anisotropy coefficients α_G, α_E and α_ν are defined as

$$\alpha_G = \frac{G_{pp}}{G_{tp}} \tag{9}$$

$$\alpha_E = \frac{E_p}{E_t} \tag{10}$$

$$\alpha_\nu = \frac{\nu_{pp}}{\nu_{tp}} \tag{11}$$

G_{ij} are shear moduli, E_i are Young moduli and ν_{ij} are Poisson ratios. Subscript "$_p$" denotes direction within the plane of isotropy (typically horisontal direction) and subscript "$_t$" denotes direction transverse to the plane of isotropy (typically vertical direction).

When compared to the reference model, incorporation of anisotropic form of $\boldsymbol{\mathcal{L}}$ requires re-evaluation of the factor f_s from (1). According to Mašín (2012c), this factor may be quantified by comparing the isotropic unloading formulation of the hypoplastic model with the isotropic unloading line of the pre-defined form

$$\frac{\dot{e}}{1+e} = -\kappa^* \frac{\dot{p}}{p} \tag{12}$$

The isotropic version of the model is obtained by algebraic manipulations with (1) (for formulation of all model components see Appendix A)

$$\dot{p} = \left(\frac{p}{\lambda^*} - 2f_s\frac{A_m}{9}\right)\frac{\dot{e}}{1+e} \tag{13}$$

where

$$A_m = \nu_{pp}^2\left(\frac{4\alpha_E}{\alpha_\nu} - 2\alpha_E^2 + 2\frac{\alpha_E^2}{\alpha_\nu^2} - 1\right) + \nu_{pp}\left(\frac{4\alpha_E}{\alpha_\nu} + 2\alpha_E\right) + 2\alpha_E + 1 \tag{14}$$

Comparison of (13) with (12) then yields

$$f_s = -\frac{3\,\mathrm{tr}\boldsymbol{\sigma}}{2A_m}\left(\frac{1}{\lambda^*} + \frac{1}{\kappa^*}\right) \tag{15}$$

The proposed model reduces to the reference one[2] for $\alpha_G = \alpha_E = \alpha_\nu = 1$.

To predict very small strain stiffness and recent stress history effects, the model must be combined with the intergranular strain concept by Niemunis and Herle (1997) (see Appendix B for its formulation). The very small strain stiffness matrix $\boldsymbol{\mathcal{M}}_0$ then reads

$$\boldsymbol{\mathcal{M}}_0 = m_R f_s \boldsymbol{\mathcal{L}} \tag{16}$$

[2] Note that additional modification of an exponent appearing in the formulation of f_d is proposed, which is detailed in Appendix A.

The shear G_{tp0} component of the tensor $\boldsymbol{\mathcal{M}}_0$ is given by (from (2), (14) and (15))

$$G_{tp0} = m_R \frac{9p}{2A_m}\left(\frac{1}{\lambda^*} + \frac{1}{\kappa^*}\right)\frac{\alpha_E}{2\alpha_G}\left(1 - \nu_{pp} - 2\frac{\alpha_E}{\alpha_\nu^2}\nu_{pp}^2\right) \tag{17}$$

In the present work, we consider the following dependency of G_{tp0} on mean stress p (Wroth and Houlsby 1985)

$$G_{tp0} = p_r A_g \left(\frac{p}{p_r}\right)^{n_g} \tag{18}$$

where A_g and n_g are parameters and p_r is a reference pressure of 1 kPa. Comparison of (17) and (18) yields the following expression[3] for the variable m_R.

$$m_R = p_r A_g \left(\frac{p}{p_r}\right)^{n_g} \frac{4A_m\alpha_G}{2p\alpha_E}\left(\frac{\lambda^*\kappa^*}{\lambda^*+\kappa^*}\right)\frac{1}{\left(1-\nu_{pp}-2\frac{\alpha_E}{\alpha_\nu^2}\nu_{pp}^2\right)} \tag{19}$$

Complete model formulation is given in Appendices. Its finite element implementation is freely available on the web Gudehus et al. (2007).

Model calibration

In this section, we focus on calibration of material constants new with respect to the original model. For calibration of the parameters parameters φ_c, N, λ^* and κ^*, the readers are referred to Mašín (2012b). As discussed by Mašín and Rott (2013), complete calibration of transversely isotropic elastic models requires five measurements of wave propagation velocities:

- $V_{SH}(0°)$: S-wave velocity propagating in the direction normal to the plane of isotropy.
- $V_{SH}(90°)$: S-wave velocity propagating within the plane of isotropy with in-plane polarisation.
- $V_P(0°)$: P-wave velocity propagating in the direction normal to the plane of isotropy.
- $V_P(90°)$: P-wave velocity propagating within the plane of isotropy.
- $V_P(45°)$: P-wave velocity under inclination of 45° with respect to the plane of isotropy.

The material constants may then be calculated using

$$G_{tp0} = E \tag{20}$$

$$\alpha_G = \frac{C-D}{2E} \tag{21}$$

$$\nu_{pp} = \frac{AD-B^2}{AC-B^2} \tag{22}$$

$$\alpha_\nu = \frac{C+D}{B}\nu_{pp} \tag{23}$$

$$\alpha_E = \frac{B\alpha_\nu^2 - C\alpha_\nu\nu_{pp}(1+\nu_{pp})}{B\nu_{pp}^2} \tag{24}$$

[3] Note that in the original intergranular strain concept formulation, m_R is considered as a parameter. Contrary, in the formulation proposed here, m_R is a variable calculated on the basis of G_{tp0} expression (18).

where (from Mavko et al. 2009)

$$C = \rho_t V_P^2(90°) \tag{25}$$
$$D = C - 2\rho_t V_{SH}^2(90°) \tag{26}$$
$$A = \rho_t V_P^2(0°) \tag{27}$$
$$E = \rho_t V_{SH}^2(0°) \tag{28}$$
$$B = -E + \sqrt{4\rho_t^2 V_P^4(45°) - 2\rho_t V_P^2(45°)(C + A + 2E) + (C + E)(A + E)} \tag{29}$$

with ρ_t being soil density.

The above mentioned experiments are not routinely performed in geotechnical engineering laboratories. A simpler calibration procedure assumes that at least bender element shear velocity measurements on vertically and horziontally oriented samples are available for calibration of α_G. α_E and α_ν may then be evaluated using empirical correlations proposed by Mašín and Rott (2013). Let us define the exponents x_{GE} and $x_{\mathrm{G\nu}}$ as

$$\alpha_E = \alpha_G^{(1/x_{GE})} \tag{30}$$
$$\alpha_\nu = \alpha_G^{(1/x_{G\nu})} \tag{31}$$

Based on evaluation of an extensive experimental database, Mašín and Rott (2013) suggested[4] x_{GE}=0.8 and $x_{G\nu} = 1$. The remaining parameter ν_{pp} may in this simplified calibration procedure be estimated by trial-and-error using large strain shear stiffness measurements.

Evaluation of the model

The proposed model has been evaluated using extensive experimental data set on London clay from Imperial College project by Nishimura et al. (2007), Nishimura (2005), Gasparre et al. (2007) and Gasparre (2005). They tested undisturbed samples of London clay from the excavation at Heathrow, Terminal 5. For the material description and details of the experimental procedures the readers are referred to the above cited publications. The parameters α_{G}, A_g and n_g were calibrated using resonant column appartus tests on London clay. Empirical expressions were adopted for α_{E} (30) and α_ν (31). ν_{pp} was estimated using stress-strain curves of shear tests at large strains. The parameters φ_c, λ^* and κ^*, calibrated using data by Gasparre (2005), were taken over from Mašín (2009). The parameter N was adjusted so that the soil overconsolidation manifested by the undrained stress paths was predicted properly. The initial value of void ratio $e = 0.69$ was calculated from the specimen water content and specific gravity provided by Nishimura et al. (2007). The material parameters adopted in all the simulations are in Table 1 and 2. Predictions by the proposed model have been compared with predictions by the reference model by Mašín (2005).

In the evaluation, we used hollow cylinder tests on London clay from the depth of 10.5m by Nishimura (2005) and Nishimura et al. (2007). Two sets of experiments have been simulated.

[4] Note that the classical Graham and Houlsby (1983) model assumes x_{GE}=0.5 and $x_{G\nu} = 1$

In the first one, the soil was isotropically consolidated to the *in-situ* effective stress of $p = 323$kPa (series "IC" by Nishimura et al. 2007). In the second one, the initial conditions represented the estimated anisotropic *in-situ* stress state of $p = 323$ kPa and $p = -166$ kPa (series "AC" by Nishimura et al. 2007). In both cases, the soil was sheared after consolidation under undrained conditions with controlled vertical strain. Total stress path was defined by constant total mean stress and constant values of variables $\alpha_{d\sigma}$and b. These were defined as

$$\alpha_{d\sigma} = \frac{1}{2}\text{atan}\left(\frac{2\Delta\tau_{z\theta}}{\Delta\sigma_z - \Delta\sigma_\theta}\right) \tag{32}$$

$$b = \frac{\sigma_2 - \sigma_3}{\sigma_1 - \sigma_3} \tag{33}$$

where σ_1, σ_2 and σ_3 are the major, intermediate and minor principal stresses respectively and σ_z, σ_θ and $\tau_{z\theta}$ are rectilinear stress components in the specimen frame of reference (see Nishimura et al. 2007). The value of b represents the contribution of the intermediate principal stress such that in the standard compression experiment in triaxial apparatus $b = 0$. Only simulations with $b = 0.5$ are presented here for brevity. $\alpha_{d\sigma}$ represents the principal stress inclination revealing soil anisotropy. In the standard triaxial test, $\alpha_{d\sigma} = 0°$ for the vertically trimmed specimen and $\alpha_{d\sigma} = 90°$ for the horizontally trimmed specimen.

Figure 1a demonstrates calibration of the parameter α_{G} and predictions of very small strain stiffness anisotropy. Figure 1b shows secant stiffness $G_{z\theta}$ degradation with shear strain $\gamma_{z\theta}$ in hollow cylinder test with $\alpha_{d\sigma} = 23°$ and $b = 0.5$ and as predicted by the model.

Stress paths of various tests are in the p vs. $(\sigma_z - \sigma_\theta)/2$ stress space plotted in Fig. 2. Stress-strain curves (q/p vs. the principal strain difference $\epsilon_1 - \epsilon_3$) are presented in Fig. 3. The soil anisotropy is revealed by the deviation of the stress path from vertical (constant p). The proposed model predicts the stress path inclination properly for both isotropically and anisotropically consolidated specimens. The stress paths deviate from the experimental after the peak of q/p, but this may be explained by the specimen rupture and strain localisation into shear bands (see Nishimura et al. 2007 for indication of the pre-rupture stress path portions). Predictions by the model by Mašín (2005) are shown in Figs. 2c and 3e,f for comparison. This model predicts some degree of stress-induced anisotropy in the anisotropically consolidated specimens, but its degree cannot be controlled by a parameter and in the present case it is clearly underestimated. The response of the isotropically consolidated specimens is incorrectly predicted as initially isotropic by the Mašín (2005) model.

Summary and conclusions

A new version of clay hypoplasticity model is developed for predicting stiffness anisotropy. The model is based on the reference model by Mašín (2012b), in which the stiffness tensor $\boldsymbol{\mathcal{L}}$ is replaced by an anisotropic elasticity tensor. The model has been evaluated using comprehensive data set on London clay, which includes measurements of the influence of anisotropy in the hollow cylinder apparatus. It is demonstrated that the proposed model predicts not only the influence of anisotropy on the very small strain stiffness, but it also improves predictions of undrained stress paths.

Acknowledgment

Financial support by the research grant P105/12/1705 of the Czech Science Foundation is greatly appreciated.

Notation and conventions

Compression negative sign convention is adopted throughout.

Tensorial operations:

$\|\mathbf{X}\|$ Euclidean norm $\sqrt{X_{ij}X_{ij}}$
tr$\mathbf{X}$ trace operator $1_{ij}X_{ij}$
$\boldsymbol{\mathcal{L}}:\mathbf{Y}$ inner product $L_{ijkl}Y_{kl}$
$\mathbf{X}\otimes\mathbf{Y}$ outer product $X_{ij}Y_{kl}$
$\mathbf{X}\cdot\mathbf{Y}$ inner product $X_{ij}Y_{jk}$
$\mathbf{X}\circ\mathbf{Y}$ tensor product $\frac{1}{2}\left(X_{ik}Y_{jl}+X_{il}Y_{jk}+X_{jl}Y_{ik}+X_{jk}Y_{il}\right)$
$\dot{X}$ rate of X
$\mathring{\mathbf{X}}$ objective (Jaumann) rate of $\mathbf{X}$
$\widehat{\mathbf{X}}$ tensor normalised by its Euclidean norm $\widehat{\mathbf{X}}=\mathbf{X}/\|\mathbf{X}\|$

Variables:

$\mathbf{1}$ second-order identity tensor
$\boldsymbol{\sigma}$ Cauchy effective stress tensor
p mean effective stress
$\dot{\boldsymbol{\epsilon}}$ Euler stretching tensor
e void ratio
$\boldsymbol{\mathcal{L}}$ hypoplasticity fourth-order tensor
$\mathbf{N}$ hypoplasticity second-order tensor
f_s barotropy factor of hypoplastic equation
f_d pyknotropy factor of hypoplastic equation
a_1, a_2, a_3, a_4, a_5 parameters of transversely isotropic elasticity model
A, B, C, D, E parameters of transversely isotropic elasticity model
$\mathbf{n}$ unit vector normal to the plane of symmetry
$\mathbf{p}$ second order tensor $p_{ij}=n_i n_j$
G_{tp}, G_{pp} shear moduli ("$_p$" in-plane direction, "$_t$" transversal direction)
E_t, E_p Young moduli ("$_p$" in-plane direction, "$_t$" transversal direction)
ν_{tp}, ν_{pp} Poisson ratios ("$_p$" in-plane direction, "$_t$" transversal direction)
α_G anisotropy ratio of shear moduli

α_E anisotropy ratio of Young moduli
α_ν anisotropy ratio of Poisson ratios
x_{GE}, $x_{G\nu}$ exponents of transversely elastic model formulation
N hypoplastic model parameter (position of normal compression line)
λ^* hypoplastic model parameter (slope of normal compression line)
κ^* hypoplastic model parameter controlling volumetric unloading response
φ_c critical state friction angle
A_m variable in hypoplastic model formulation
$\boldsymbol{\mathcal{M}}_0$ very small strain stiffness tensor
m_R variable controlling very small strain shear modulus
G_{tp0} shear modulus at very small strain
p_r reference stress equal to 1 kPa
A_g parameter quantifying the dependency of G_{tp0} on mean stress
n_g parameter quantifying the dependency of G_{tp0} on mean stress
$V_{SH}(X°)$ S-wave velocity (X is the direction of propagation with respect to the axis of symmetry)
$V_P(X°)$ P-wave velocity (X is the direction of propagation with respect to the axis of symmetry)
ρ_t soil density
$\alpha_{d\sigma}$ principal stress increment inclination in hollow cylinder test
ΔX Finite increment of X
σ_1, σ_2, σ_3 principal stresses (major, intermediate, minor)
ϵ_1, ϵ_3 principal strains (major, minor)
σ_z, σ_θ, $\tau_{z\theta}$ rectilinear stress components in the specimen frame of reference in hollow cylinder apparatus
b variable quantifying the intermediate principal stress magnitude in hollow cylinder apparatus

Hypoplasticity specific variables (appearing in appendices only):

f_d^A pyknotropy factor of hypoplastic equation, asymptotic state value
$\boldsymbol{\mathcal{A}}$ fourth-order tensor in hypoplastic model formulation
p_e Hvorslev equivalent pressure
$\mathbf{d}^A$ second-order tensor specifying asymptotic strain rate direction
$\mathbf{d}$ normalised second-order tensor specifying asymptotic strain rate direction
α_f hypoplastic variable controlling rate of stiffness decrease, may be considered as a model parameter
F_m factor of Matsuoka-Nakai yield condition
ω variable controlling asymptotic state boundary surface shape
a hypoplastic variable controlling peak strength, which may be considered as a model parameter
I_1, I_2, I_3 stress invariants
$\cos 3\theta$ Lode angle function
ξ variable controlling asymptotic strain rate direction
a_f variable in hypoplastic model formulation
R, m_{rat}, β_r, χ intergranular strain concept parameters

$\boldsymbol{\mathcal{M}}$ stiffness tensor of the intergranular strain concept formulation
m_T variable in the intergranular strain concept formulation
$\boldsymbol{\mathcal{I}}$ fourth-order identity tensor
$\boldsymbol{\delta}$ intergranular strain tensor
ρ normalised intergranular strain tensor magnitude
$\mathbf{0}$ second-order null tensor

Appendix A

The Appendix summaries remaining equations of the proposed hypoplastic model which have not been specified in the main text.

$$\mathring{\boldsymbol{\sigma}}= f_s\boldsymbol{\mathcal{L}} : \dot{\boldsymbol{\epsilon}} - \frac{f_d}{f_d^A}\boldsymbol{\mathcal{A}} : \mathbf{d}\|\dot{\boldsymbol{\epsilon}}\| \tag{34}$$

$$\boldsymbol{\mathcal{A}} = f_s\boldsymbol{\mathcal{L}}+\frac{\boldsymbol{\sigma}}{\lambda^*}\otimes\mathbf{1} \tag{35}$$

$$f_d = \left(\frac{2p}{p_e}\right)^{\alpha_f} \tag{36}$$

$$p_e=p_r\exp\left[\frac{N-\ln(1+e)}{\lambda^*}\right] \tag{37}$$

$$f_d^A = 2^{\alpha_f}(1-F_m)^{\alpha_f/\omega} \tag{38}$$

$$F_m = \frac{9I_3+I_1I_2}{I_3+I_1I_2} \tag{39}$$

$$\omega = -\frac{\ln(\cos^2\varphi_c)}{\ln 2} + a(F_m - \sin^2\varphi_c) \tag{40}$$

$$I_1 = \operatorname{tr}\boldsymbol{\sigma} \tag{41}$$
$$I_2 = \frac{1}{2}[\boldsymbol{\sigma}:\boldsymbol{\sigma} - (I_1)^2] \tag{42}$$
$$I_3 = \det\boldsymbol{\sigma} \tag{43}$$

$$\mathbf{d} = \frac{\mathbf{d}^A}{\|\mathbf{d}^A\|} \tag{44}$$

$$\mathbf{d}^A = -\hat{\boldsymbol{\sigma}}^* + \mathbf{1}\left[\frac{2}{3} - \frac{\cos 3\theta+1}{4}(F_m)^{1/4}\right]\frac{(F_m)^{\xi/2}-\sin^{\xi}\varphi_c}{1-\sin^{\xi}\varphi_c} \tag{45}$$

$$\cos 3\theta = -\sqrt{6}\frac{\operatorname{tr}(\hat{\boldsymbol{\sigma}}^*\cdot\hat{\boldsymbol{\sigma}}^*\cdot\hat{\boldsymbol{\sigma}}^*)}{[\hat{\boldsymbol{\sigma}}^*:\hat{\boldsymbol{\sigma}}^*]^{3/2}} \tag{46}$$

$$\xi = 1.7 + 3.9\sin^2\varphi_c \tag{47}$$

$$\hat{\boldsymbol{\sigma}}^* = \frac{\boldsymbol{\sigma}}{\operatorname{tr}\boldsymbol{\sigma}} - \frac{\mathbf{1}}{3} \tag{48}$$

The exponent α_f controls irreversibility of the deformation inside the asymptotic state boundary surface. In fact, for high values of α_f the response of the basic model is practically reversible inside the asymptotic state boundary surface with $f_s\boldsymbol{\mathcal{L}}$ being the stiffness matrix. The model predictions then resemble predictions by the critical state elasto-plastic models. In the reference model by Mašín (2012b), a fixed value of $\alpha_f = 2$ has been suggested. Thorough evaluation of the model non-linear properties, however, indicated that α_f value by the Mašín (2005) model leads to better predictions. It is thus suggested to use

$$\alpha_f = \frac{\ln\left[\frac{\lambda^*-\kappa^*}{\lambda^*+\kappa^*}\left(\frac{3+a_f^2}{a_f\sqrt{3}}\right)\right]}{\ln 2} \tag{49}$$

$$a_f = \frac{\sqrt{3}(3-\sin\varphi_c)}{2\sqrt{2}\sin\varphi_c} \tag{50}$$

In fact, if needed, α_f can be considered as a model parameter controlling non-linear response inside the asymptotic state boundary surface in the case ν_{pp} is calibrated rigorously using wave velocity measurements. The model assumes parameters φ_c, λ^*, κ^*, N and ν_{pp} and state variable e (void ratio). a is controlling peak friction angle, standard value of $a = 0.3$ was suggested by Mašín (2012b). If required, the value of a can be modified to control peak friction angle, see Mašín (2012b) for details. α_G, α_E and α_ν are parameters controlling stiffness anisotropy; α_E and α_ν may be approximated using empirical formulations.

Appendix B

In this appendix, we summarise the version of the intergranular strain concept used in the proposed model. The intergranular strain concept was originally proposed by Niemunis and Herle (1997).

$$\mathring{\boldsymbol{\sigma}} = \boldsymbol{\mathcal{M}} : \dot{\boldsymbol{\epsilon}} \tag{51}$$

$$\boldsymbol{\mathcal{M}} = [\rho^\chi m_T + (1-\rho^\chi)m_R]f_s\boldsymbol{\mathcal{L}} + \begin{cases} \rho^\chi(1-m_T)f_s\boldsymbol{\mathcal{L}}:\hat{\boldsymbol{\delta}}\otimes\hat{\boldsymbol{\delta}} + \rho^\chi f_s f_d \mathbf{N}\hat{\boldsymbol{\delta}} & \text{for } \hat{\boldsymbol{\delta}}:\dot{\boldsymbol{\epsilon}} > 0 \\ \rho^\chi(m_R-m_T)f_s\boldsymbol{\mathcal{L}}:\hat{\boldsymbol{\delta}}\otimes\hat{\boldsymbol{\delta}} & \text{for } \hat{\boldsymbol{\delta}}:\dot{\boldsymbol{\epsilon}} \le 0 \end{cases} \tag{52}$$

$$\rho = \frac{\|\boldsymbol{\delta}\|}{R} \tag{53}$$

$$\hat{\boldsymbol{\delta}} = \begin{cases} \boldsymbol{\delta}/\|\boldsymbol{\delta}\| & \text{for } \boldsymbol{\delta} \neq \mathbf{0} \\ \mathbf{0} & \text{for } \boldsymbol{\delta} = \mathbf{0} \end{cases} \tag{54}$$

$$\mathring{\boldsymbol{\delta}} = \begin{cases} \left(\boldsymbol{\mathcal{I}} - \hat{\boldsymbol{\delta}}\otimes\hat{\boldsymbol{\delta}}\rho^{\beta_r}\right):\dot{\boldsymbol{\epsilon}} & for\ \hat{\boldsymbol{\delta}}:\dot{\boldsymbol{\epsilon}} > 0 \\ \dot{\boldsymbol{\epsilon}} & for\ \hat{\boldsymbol{\delta}}:\dot{\boldsymbol{\epsilon}} \le 0 \end{cases} \tag{55}$$

$$m_R = p_r A_g \left(\frac{p}{p_r}\right)^{n_g} \frac{4A_m\alpha_G}{2p\alpha_E}\left(\frac{\lambda^*\kappa^*}{\lambda^*+\kappa^*}\right)\frac{1}{\left(1-\nu_{pp}-2\frac{\alpha_E}{\alpha_\nu^2}\nu_{pp}^2\right)} \tag{56}$$

$$m_T = m_{rat} m_R \tag{57}$$

$A_g,\ n_g,\ m_{rat},\ \beta_r,\ \chi$ are parameters and $\boldsymbol{\delta}$ is state variable.

References

Addenbrooke, T., D. Potts, and A. Puzrin (1997). The influence of pre-failure soil stiffness on the numerical analysis of tunnel construction. *Géotechnique 47* (3), 693–712.

Atkinson, J. H., D. Richardson, and S. E. Stallebrass (1990). Effects of recent stress history on the stiffness of overconsolidated soil. *Géotechnique 40* (4), 531–540.

Franzius, J. N., D. M. Potts, and J. B. Burland (2005). The influence of soil anisotropy and K_0 on ground surface movements resulting from tunnel excavation. *Géotechnique 55* (3), 189–199.

Gasparre, A. (2005). *Advanced laboratory characterisation of London Clay*. Ph. D. thesis, University of London, Imperial College of Science, Technology and Medicine.

Gasparre, A., S. Nishimura, N. A. Minh, M. R. Coop, and R. J. Jardine (2007). The stiffness of natural London Clay. *Géotechnique 57* (1), 33–47.

Graham, J. and G. T. Houlsby (1983). Anisotropic elasticity of a natural clay. *Géotechnique 33* (2), 65–180.

Gudehus, G. (1996). A comprehensive constitutive equation for granular materials. *Soils and Foundations 36* (1), 1–12.

Gudehus, G., A. Amorosi, A. Gens, I. Herle, D. Kolymbas, D. Mašín, D. Muir Wood, R. Nova, A. Niemunis, M. Pastor, C. Tamagnini, and G. Viggiani (2008). The soilmodels.info project. *International Journal for Numerical and Analytical Methods in Geomechanics 32* (12), 1571–1572.

Gudehus, G. and D. Mašín (2009). Graphical representation of constitutive equations. *Géotechnique 59* (2), 147–151.

Gunn, M. J. (1993). The prediction of surface settlement profiles due to tunnelling. In G. T. Houlsby and A. N. Schofield (Eds.), *Predictive soil mechanics: Proceedings of the Worth Memorial Symposium, London*, pp. 304–316. Thomas Telford, London.

Kopito, D. and A. Klar (2013). Discussion: Hypoplastic Cam-clay model. D. Mašín (2012) Géotechnique 62, No. 6, 549-553. *Géotechnique 63* (10), 889–890.

Lubarda, V. A. and M. C. Chen (2008). On the elastic moduli and compliences of transversely isotropic and orthotropic materials. *Journal of Mechanics of Materials and Structures 3* (1), 153–171.

Mavko, G., T. Mukerji, and J. Dvorkin (2009). *The Rock Physics Handbook: tools for seismic analysis of porous media* (2nd ed.). Cambridge University Press, New York.

Mašín, D. (2005). A hypoplastic constitutive model for clays. *International Journal for Numerical and Analytical Methods in Geomechanics 29* (4), 311–336.

Mašín, D. (2009). 3D modelling of a NATM tunnel in high K_0 clay using two different constitutive models. *Journal of Geotechnical and Geoenvironmental Engineering ASCE 135* (9), 1326–1335.

Mašín, D. (2012a). Asymptotic behaviour of granular materials. *Granular Matter 14* (6), 759–774.

Mašín, D. (2012b). Clay hypoplasticity with explicitly defined asymptotic states. *Acta Geotechnica 8* (5), 481–496.

Mašín, D. (2012c). Hypoplastic Cam-clay model. *Géotechnique 62* (6), 549–553.

Mašín, D. and J. Rott (2013). Small strain stiffness anisotropy of natural sedimentary clays: review and a model. *Acta Geotechnica, DOI:10.1007/s11440-013-0271-2*.

Ng, C. W. W., E. H. Y. Leung, and C. K. Lau (2004). Inherent anisotropic stiffness of weathered geomaterial and its influence on ground deformations around deep excavations. *Canadian Geotechnical Journal 41*, 12–24.

Niemunis, A. and I. Herle (1997). Hypoplastic model for cohesionless soils with elastic strain range. *Mechanics of Cohesive-Frictional Materials 2*, 279–299.

Nishimura, S. (2005). *Laboratory study on anisotropy of natural London clay*. Ph. D. thesis, University of London, Imperial College of Science, Technology and Medicine.

Nishimura, S., N. A. Minh, and R. J. Jardine (2007). Shear strength anisotropy of natural London Clay. *Géotechnique 57* (1), 49–62.

Spencer, A. J. M. (1982). The formulation of constitutive equation for anisotropic solids. In J. P. Boehler (Ed.), *Mechanical behaviour of anisotropic solids*. Martinus Nijhoff Publishers, The Hague.

von Wolffersdorff, P. A. (1996). A hypoplastic relation for granular materials with a predefined limit state surface. *Mechanics of Cohesive-Frictional Materials 1*, 251–271.

Wroth, C. and G. Houlsby (1985). Soil mechanics - property characterisation, and analysis procedures. In *Proc.* 11th *Conf. Soil. Mech., San Francisco*, Volume 1, pp. 1–55.

Tables

Table 1: Parameters of the intergranular strain concept by Niemunis and Herle (1997) adopted in combination with different hypoplastic models.

	A_g or m_R	n_g	m_{rat} or m_T	R	β_r	χ
proposed model	$A_g = 270$	1	$m_{rat} = 0.5$	5×10^{-5}	0.08	0.9
Mašín (2005) model	$m_R = 8$	n/a	$m_T = 4$	5×10^{-5}	0.08	0.9

Table 2: Parameters of the hypoplastic models used in simulations.

	φ_c	λ^*	κ^*	N	ν_{pp} or r	α_G
proposed model	21.9º	0.095	0.015	1.19	$\nu_{pp} = 0.1$	2
Mašín (2005) model	21.9º	0.095	0.015	1.19	$r = 0.3$	n/a

Figure captions

Figure 1: (a) α_G calibration based on experiments by Nishimura (2005) and Gasparre (2005). (b) Secant shear stiffness degradation as measured by Nishimura (2005) in hollow cylinder test with $\alpha_{d\sigma} = 23°$ and $b = 0.5$ and predictions by the proposed model.

Figure 2: Stress paths in the p vs. $(\sigma_z - \sigma_\theta)/2$ stress space: Experimental data by Nishimura et al. (2007), proposed model and Mašín (2005) model predictions.

Figure 3: The ratio q/p vs. the principal strain difference $\epsilon_1 - \epsilon_3$ for three simulation sets: Experimental data by Nishimura et al. (2007), proposed model and Mašín (2005) model predictions.

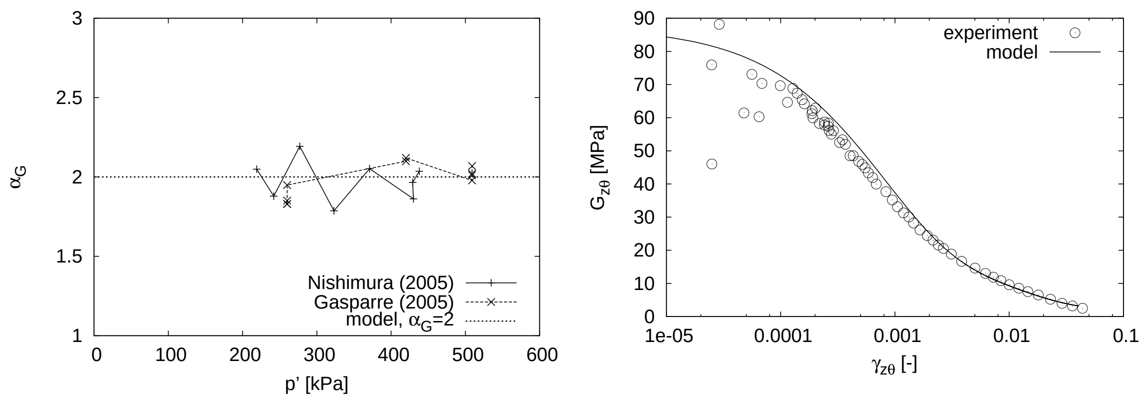

(a) (b)

Figure 1: (a) α_G calibration based on experiments by Nishimura (2005) and Gasparre (2005). (b) Secant shear stiffness degradation as measured by Nishimura (2005) in hollow cylinder test with $\alpha_{d\sigma} = 23°$ and $b = 0.5$ and predictions by the proposed model.

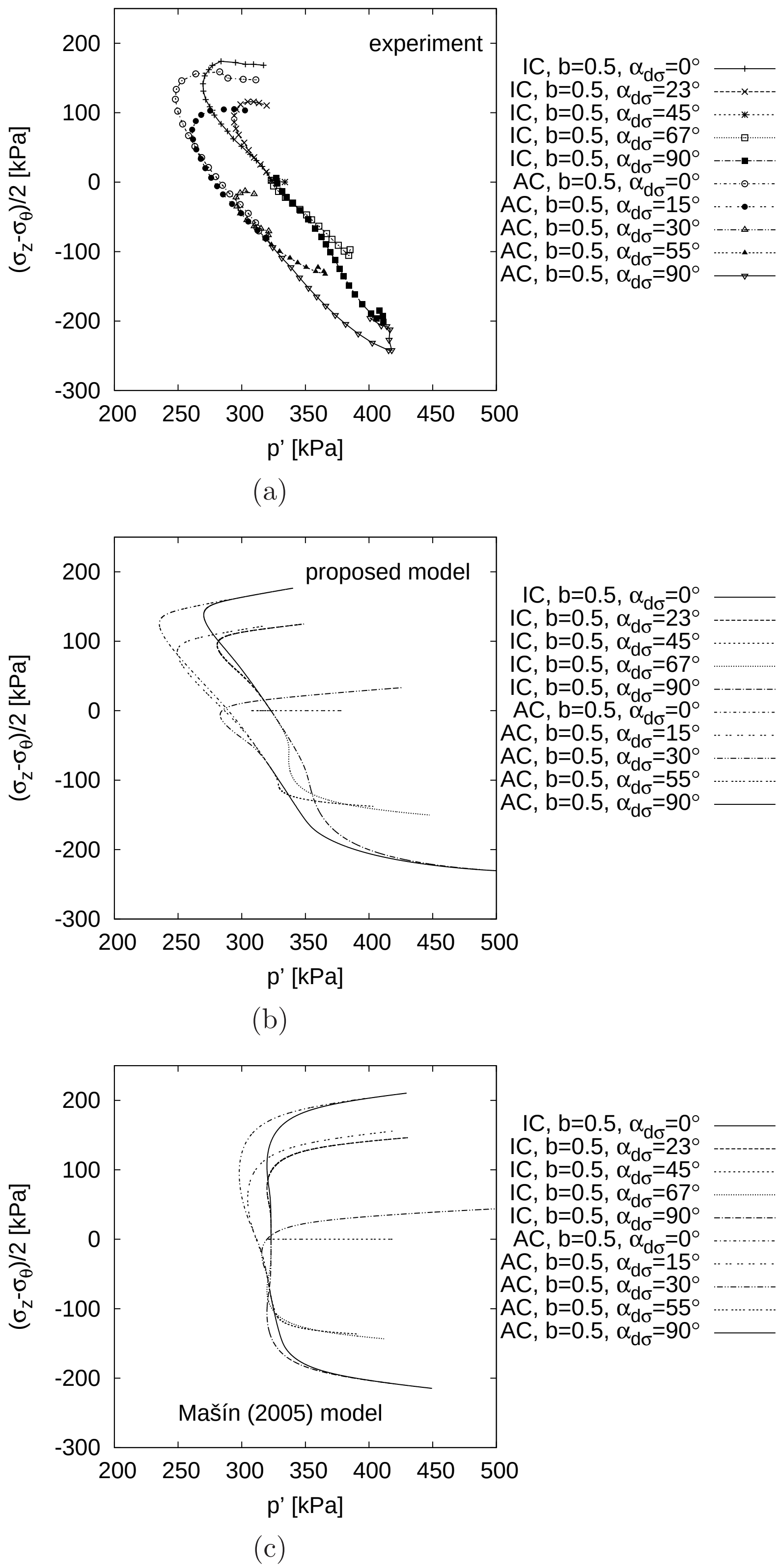

Figure 2: Stress paths in the p' vs. $(\sigma_z - \sigma_\theta)/2$ stress space: Experimental data by Nishimura et al. (2007), proposed model and Mašín (2005) model predictions.

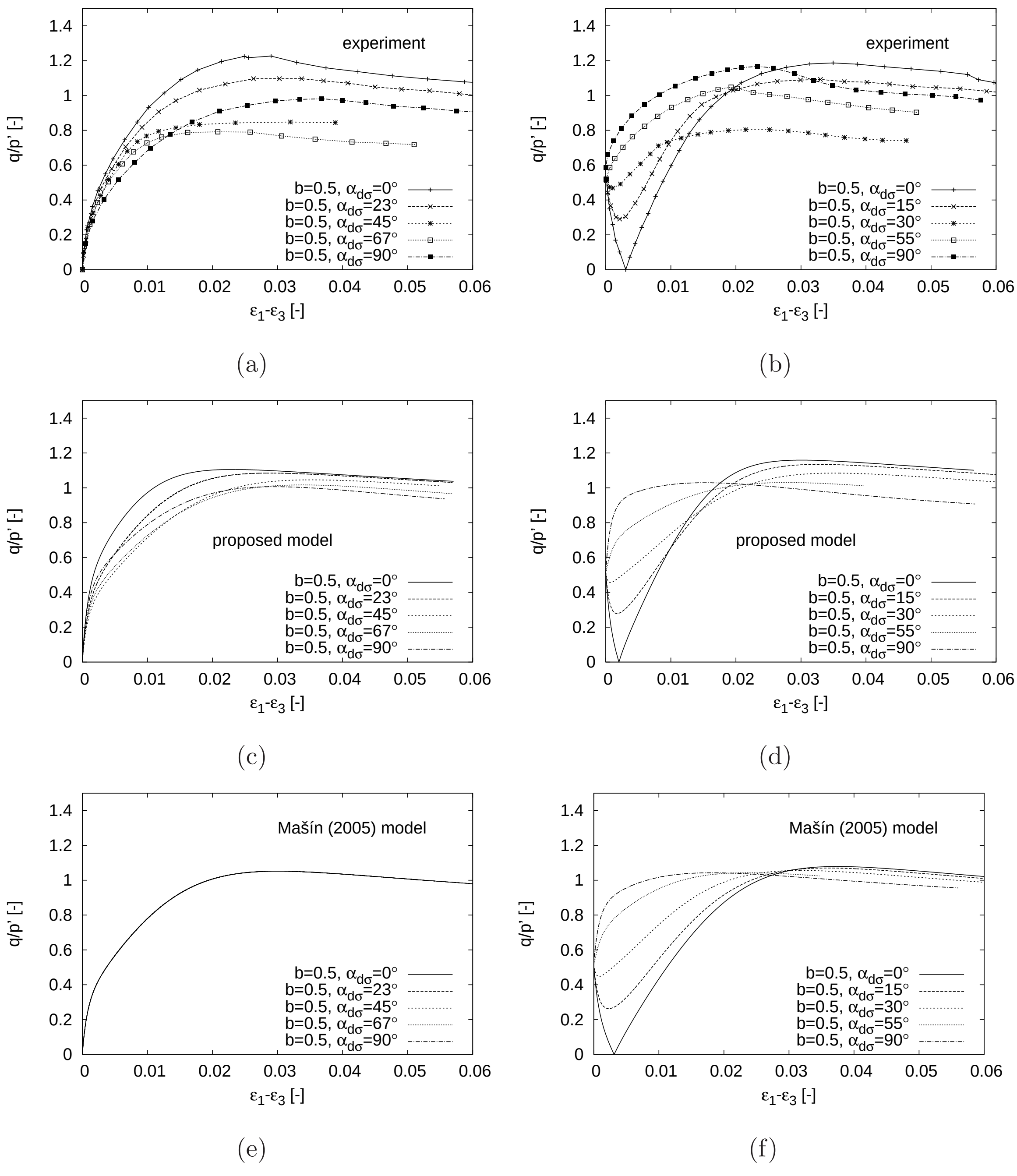

Figure 3: The ratio q/p' vs. the principal strain difference $\epsilon_1 - \epsilon_3$ for three simulation sets: Experimental data by Nishimura et al. (2007), proposed model and Mašín (2005) model predictions.